Supporting Online Material for

Multifunctional Nanomechanical Systems via Tunably Coupled Piezoelectric Actuation

Sotiris C. Masmanidis, Rassul B. Karabalin, Iwijn De Vlaminck, Gustaaf Borghs, Mark R. Freeman, Michael L. Roukes*

*To whom correspondence should be addressed. E-mail: roukes@caltech.edu

Published 10 August 2007, *Science* **317**, 780 (2007)
DOI: 10.1126/science.1144793

This PDF file includes:

Supporting Material

Multifunctional Nanomechanical Systems via Tunably-coupled Piezoelectric Actuation

S. C. Masmanidis, R. B. Karabalin, I. De Vlaminck, G. Borghs, M. R. Freeman, M. L. Roukes

I. Materials & Methods

A. Epitaxial *pin* diode structures

The material is grown on a p^+ GaAs (001) substrate using molecular beam epitaxy. A sacrificial layer of 550 nm of p-$Al_{0.8}Ga_{0.2}As$ (10^{18} cm^{-3}) is deposited, followed by the 200 nm p-type/intrinsic/n-type (*pin*) heterostructure with the p-type layer on the bottom. Three separate wafers are grown with the following thickness and doping specifications (doping in cm^{-3}). Diode *pin*-1: 100 nm n-GaAs (10^{19}) / 50 nm i-GaAs / 50 nm p-GaAs (10^{18}); *pin*-2: 100 nm n-GaAs (10^{19}) / 50 nm i-GaAs / 50 nm p-GaAs (10^{19}); *pin*-3: 50 nm n-GaAs (10^{19}) / 50 nm i-GaAs / 100 nm p-GaAs (10^{18}). Note that the intrinsic layers referred to as i-GaAs have a p-type background concentration of ~$5x10^{15}$ cm^{-3}, however, this is negligible compared to the intentionally doped n and p-type regions.

B. NEMS device fabrication

For the top electrical contact, 150X150 μm^2 electrodes are defined photolithographically and deposited with a thin Ti adhesion layer followed by 50 nm of Au. Low contact resistance is obtained without annealing. The large electrode area was necessary for wedge-type wirebonding of Au contact wires. For the bottom contact the back side of the p^+ wafer is covered with Ti/Au. Electron-beam lithography is used to define a NEMS device adjacent to the top electrode. A 70 nm Ti etching mask is evaporated in the developed pattern, and is followed by a low energy Ar ion milling step to remove the unmasked *pin* layer. Finally, the preferential etching of $Al_{0.8}Ga_{0.2}As$ to GaAs by dilute hydrofluoric acid allows the devices to be released from the substrate, and HF simultaneously removes any remaining Ti masking material. Electrical connection to the bottom contact is maintained through unetched, highly doped AlGaAs underneath the large electrodes. The cantilevers and doubly clamped beam (Figs. 1 and 3 in the main text, respectively) both have dimensions (L, w, t)=(4, 0.8, 0.2) μm. The 0.8 μm width was chosen to provide a large reflected optical signal. The doubly clamped beam is fabricated from the *pin*-1 heterostructure. The L-shaped structure (Fig. 4 in the main text, constructed from the *pin*-1 heterostructure) has two arms that are 3.8 μm long and 0.5 μm wide. Prior to selectively removing the AlGaAs in that device, the top 130 nm was removed by ion milling from the corner where the arms meet, leaving two electrically isolated but mechanically connected terminals.

C. Optical measurement

Samples are mounted in a room temperature vacuum (P=5 mTorr) chamber fitted with a sapphire optical window. The bottom electrode is grounded. In order to minimize the impact of light on device performance (heating, photocarrier generation) a 2 mW, 904 nm infrared laser diode is used with a 10-fold extinction factor neutral density filter. The beam is focused to a spot of 10-20 μm diameter. A low noise, high bandwidth photoreceiver is used for detection. Optical signals

are converted into displacement by one of the following three methods. (i) The resonance amplitudes of the cantilever in Figs. 1C and 2A are calibrated to the thermomechanical noise amplitude at room temperature, which can be calculated using the expressions in Ref. S1. However, thermomechanical noise measurements are not available for the stiffer devices shown in Figs. 3 and 4. (ii) The doubly-clamped beam in Fig. 3A is calibrated by measuring the onset of nonlinear mechanical bistability, which was found to occur at a drive of 330 mV for the 4 μm-long doubly-clamped beam with the Q of 700. This value (330 mV) is then normalized with respect to the critical amplitude $z_{crit} \approx t\sqrt{4.19/Q}$, which is derived from Ref. S2. (iii) The amplitude of the L-shaped cantilever in Fig. 4A is estimated from the model of piezoelectric actuation that is discussed below. Note: all ac driving voltages refer to root-mean-square (rms) values.

II. Supporting Text

In this section we obtain approximate expressions for the tunable piezoelectric actuation of a cantilever responsible for the effects observed in Fig. 2 from the main text.

Mechanism 1 - depletion-mediated strain:

The static, out of plane deflection of a trimorph cantilever is (see Ref. S3):

$$z(V) = (3L^2 d_{3j} V / t_{tot}^4)\left\{t_n(V)[t_n(V) + t_m(V)] - t_p(V)[t_p(V) + t_m(V)]\right\} \quad \text{(S1)}$$

where L is the cantilever's length, d_{3j} is the piezoelectric constant, V is voltage and t_{tot}=200 nm. The bias-dependent *n*, *p* and middle (*i.e.,* intrinsic) layer thickness are denoted by $t_n(V)$, $t_p(V)$ and $t_m(V)$ respectively. Piezoelectric strain originates within $t_m(V)$. In the abrupt junction approximation the depletion width of a *pin* diode is

$$d(V) = \sqrt{t_{m,0}^2 + 2\varepsilon N_{tot}(V_{bi} - V)/eN_A N_D} \quad \text{(S2)}$$

where $t_{m,0}$ is the as-grown intrinsic layer thickness, N_A and N_D is the respective *p* and *n* layer doping concentration, and ε is the dielectric constant. The doping impurities are assumed to be fully ionized at room temperature. This model breaks down in the vicinity of the built-in potential V_{bi}~1.2 volts, and we restrict our analysis to below this value. The electric field distribution in the *pin* junction drops linearly from a maximum at the intrinsic layer to zero at the edges of the charge depletion region. Most of the electric field, hence most of the piezoelectric strain, is concentrated within the half-maximum points, yielding the following approximation for layer thicknesses:

$$t_p(V) = t_{p,0} - 0.5N_D[d(V) - t_{m,0}]/N_{tot}$$
$$t_m(V) = t_{m,0} + 0.5d(V) \quad \text{(S3A, B, C)}$$
$$t_n(V) = t_{n,0} - 0.5N_A[d(V) - t_{m,0}]/N_{tot}$$

The resonant motion is effectively amplified by the quality factor Q, such that the resonance amplitude is given by

$$A(V_{DC}, v_{AC}) = 0.5Q\left|z(V_{DC} + v_{AC}) - z(V_{DC} - v_{AC})\right| \quad \text{(S4)}$$

Equations S1 and S4 are plotted as a function of voltage in Fig. S1.

Mechanism 2 – variable impedance of *pin* junction:

The diode's resistance R_d and junction capacitance C_j will depend on applied voltage, so under large bias/high frequency conditions a sizeable fraction of the radio frequency driving signal v_{AC}

will be attenuated. The model for signal attenuation effects is based on the equivalent circuit of diode-embedded resonators, depicted in Fig. S2A. A *pin* diode can be treated as a variable resistance and junction capacitance in parallel, and in series with the resistance of the contacts and intrinsic layer. The motional LCR components are found to have a negligible impact on electrical properties and are henceforth ignored. The entire circuit is in series with a contact electrode and other external impedances denoted by R_0, which are on the order of 50 Ω. As long as the total diode impedance greatly exceeds R_0, most of the driving voltage will contribute toward piezoelectric actuation. The actuation efficiency as a function of dc bias is given by

$$v_{AC} / v_{AC,0} \approx R_d / \sqrt{(R_0 + R_d)^2 + (\omega R_0 R_d C_j)^2} \qquad \text{(S5)}$$

The diode resistance and capacitance are respectively given by $R_d(V)=dV/dI$ and $C_j(V)=\varepsilon A/d(V)$, where A is the contact electrode plus mechanical device area, and equal to 150x150 μm^2 in this set of devices. The I(V) curves of the three *pin* diodes are displayed in Fig. S2B. The corresponding ac driving efficiencies calculated from Eqn. S5 are plotted in Fig. S2C. The model shown in the inset of Fig. 2C (main text) is obtained by multiplying the curves in Figs. S1B and S2C, and normalizing the amplitudes with respect to their zero dc bias value.

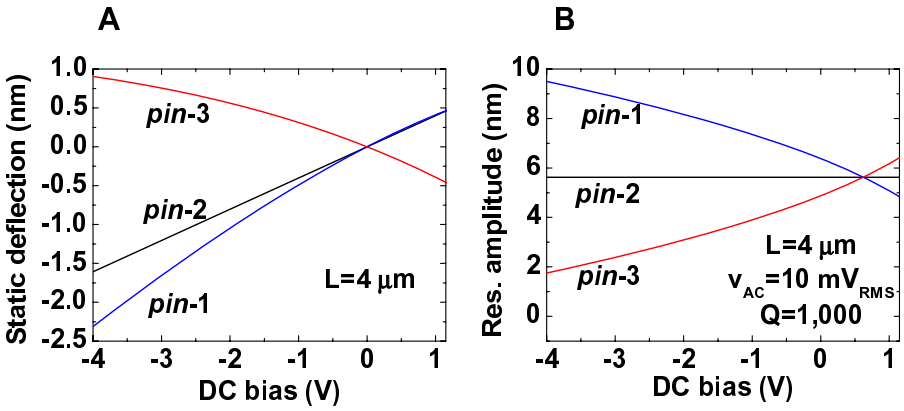

Fig. S1. Effect of depletion-mediated strain on the actuation of a piezoelectric NEMS resonator. **(A)** Plot of Eqn. S1; static deflection given a 4 μm-long cantilever. **(B)** Plot of Eqn. S4; resonance amplitude of a 4 μm cantilever assuming a Q=1,000 and drive of 10 mV_{RMS}.

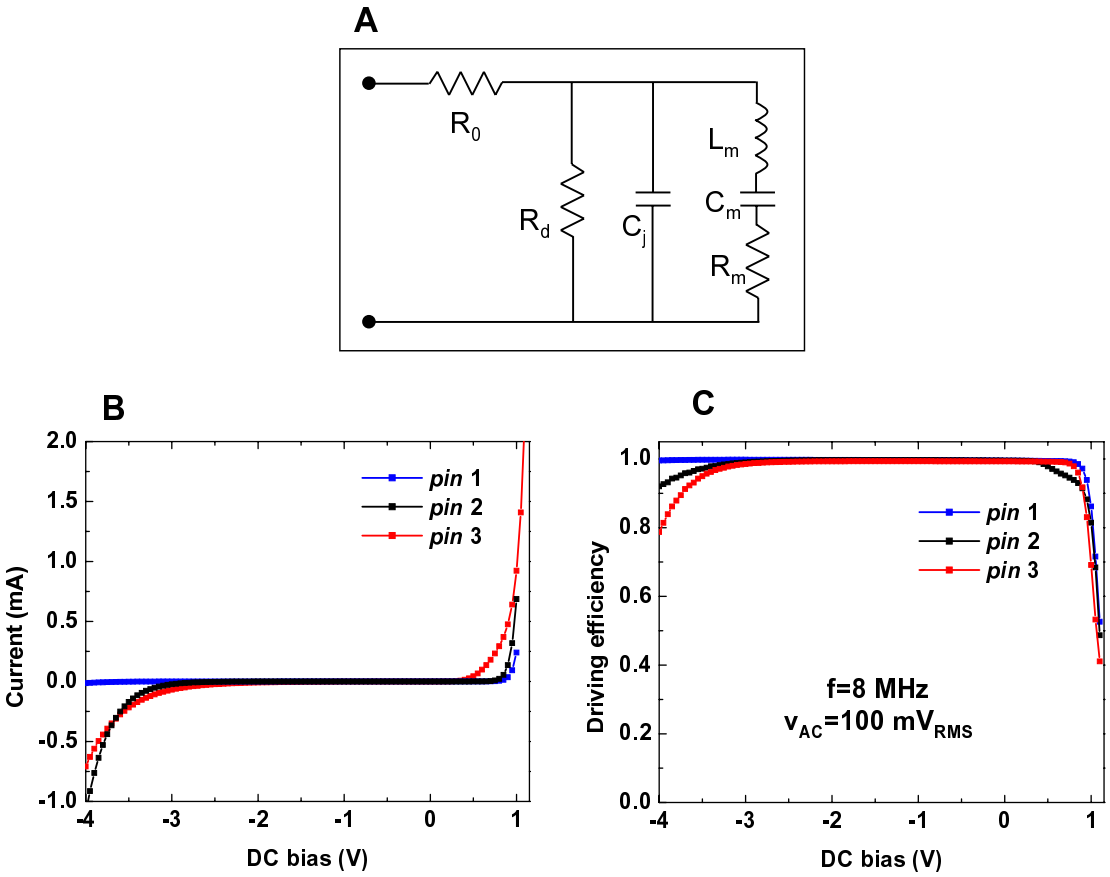

Fig. S2. (A) Equivalent circuit of mechanical *pin* diode resonator. R_0, $R_d(V)$, $C_j(V)$ are the contact resistance, diode resistance and junction capacitance, respectively. The estimated motional circuit components have ~100 times higher impedance than other components, and can thus be neglected in the analysis. **(B)** Measured I(V) curves of the three *pin* diodes and **(C)** the calculated driving efficiency of a 8 MHz signal using Eqn. S5. The efficiency from -3 to 0.7 V is very close to 100% for all three diodes.

IV. References

S1. A. N. Cleland, M. L. Roukes, *J. Appl. Phys.* **92**, 2758 (2002).

S2. H. A. Tilmans, M. Elwenspoek, J. H. J. Fluitman, *Sens. Actuat. A* **30**, 35 (1992).

S3. J. Soderkvist, *J. Micromech. Microeng.* **3**, 24 (1993).